Research Article

Muhammad Imran Asjad*, Muhammad Usman, Muhammad Madssar Kaleem, Dumitru Baleanu, and Taseer Muhammad

Thermal transport with nanoparticles of fractional Oldroyd-B fluid under the effects of magnetic field, radiations, and viscous dissipation: Entropy generation; *via* finite difference method

https://doi.org/10.1515/phys-2022-0166
received February 14, 2022; accepted May 30, 2022

Abstract: It is a well-known fact that functional effects like relaxation and retardation of materials, and heat transfer phenomena occur in a wide range of industrial and engineering problems. In this context, a mathematical model is developed in the view of Caputo fractional derivative for Oldroyd-B nano-fluid. Nano-sized particles of copper (Cu) are used to prepare nano-fluid taking water as the base fluid. The coupled non-linear governing equations of the problem are transformed into dimensionless form. Finite difference scheme is developed and applied successfully to get the numerical solutions of deliberated problem. Influence of different physical parameters on fluid velocity profile and temperature profile are analyzed briefly. It is observed that for increasing values of fractional parameter (α), fluid velocity increased, but opposite behavior was noticed for temperature profile. Nusselt number (Nu) decayed for advancement in values of heat source/sink parameter (Q_0), radiation parameter (Nr), volume fraction parameter of nano-fluid (ϕ), and viscous dissipation parameter (Ec). Skin friction (C_f) boosts for the increase in the values of magnetic field parameter (Ha). It can also be noticed that the extended finite difference scheme is an efficient tool and gives the accurate results of discussed problem. It can be extended for more numerous type heat transfer problems arising in physical nature with complex geometry.

Keywords: Oldroyd-B nano-fluid, Caputo time fractional model, viscous dissipation, thermal radiations, magnetic field, finite difference method

* **Corresponding author: Muhammad Imran Asjad,** Department of Mathematics, University of Management and Technology, Lahore, 54770, Pakistan, e-mail: Imran.asjad@umt.edu.pk
Muhammad Usman: School of Mathematical Sciences, Jiangsu University, Zhenjiang 212013, China
Muhammad Madssar Kaleem: Department of Mathematics, University of Management and Technology, Lahore, 54770, Pakistan
Dumitru Baleanu: Department of Mathematics, Cankaya University, Balgat, Ankara, Turkey; Institute of Space Sciences, 06530 Bucharest, Romania; Department of Medical Research, China Medical University Hospital, China Medical University, Taichung, Taiwan
Taseer Muhammad: Department of Mathematics, College of Sciences, King Khalid University, Abha 61413, Saudi Arabia

Nomenclature

u (m/s)	velocity
θ (K)	temperature
ρ_{nf} (kg/m^3)	density
μ_{nf} (kg/ms)	dynamic viscosity
k_{nf} (W/m K)	thermal conductivity of nano-fluid
β_θ (K^{-1})	volumetric thermal expansion coefficient
g (m/s^2)	gravitational acceleration
$(C_p)_{nf}$	heat capacity of nanoparticles
σ_{nf} (S/m)	electrical conductivity of nanoparticles
ν_{nf} (m^2/s)	kinematic viscosity of nanoparticles
ϕ	volume fraction of nanoparticles

1 Introduction

In the modern era of science and technologies, a lot of researchers are engrossing by the non-Newtonian fluids because non-Newtonian fluids have much more

applications then Newtonian fluids. Practically, precise forecasting of all connected features for such fluids is not credible through a single model because in non-Newtonian fluids, shear stress and shear rate are nonlinearly correlated to each other. Classical Navier–Stokes equation are effectual in characterizing numerous rheological properties and dynamics of these fluids, for *e.g.*, stress differences, retardation, relaxation, elongation, yield stress, memory effects, and many others. A number of different models are suggested to incorporate the additional non-linear terms and to speculate the rheological properties of non-Newtonian fluids. Certain models which explained the non-Newtonian behavior of fluids are Maxwell model [1], Sisko's model [2], Second grade fluid model [3], Burgers model [4], Jeffrey model [5], and Oldroyd-B model [6]. Many non-Newtonian fluids are present in foods like jams, mayonnaise, toothpaste, polymers, clay, and melts which enumerate the elastic feature. The Oldroyd-B model is a more appropriate and amenable model to manifest the elastic and viscous nature of the fluids because it has the ability to demonstrate the flow history and it discloses the retardation and relaxation mechanism. When the value of solvent viscosity is zero, then the Maxwell model is a limiting case of Oldroyd-B model. A considerable work in mathematical modeling of blood flow through restenosis arteries has been done in bio-science by Ali *et al.* [7]. A lot of contribution in this perspective can be seen in refs [7–10]. Fetecau *et al.* [11] elaborated apposite stress field for Oldroyd-B and fluid velocity distribution over a constantly moving plate. Fetecau *et al.* [12] extended this work further more for an Oldroyd-B flow model within a channel and found the analytical solution of the proposed model. Gul [13] solved the magnetohydrodynamic (MHD) flow of Oldroyd-B fluid model past an oscillating belt analytically by Homotopy perturbation method (HPM). Wang [14] scrutinized the dissipative non-linear flow of Oldroyd-B fluid generated by stretchable sheet *via* HPM. Song [15] elaborated the fractional Oldroyd-B model analytically *via* fluctuating duct. Hayat [16] investigated the nano-material stagnation point flow of Oldroyd-B model *via* optimal homotopy asymptotic method.

Applications of nano-fluids have become a topic of global interest for the last few decades because of their effective mode heat transfer ability. Choi and Eastman [17] in 1995, first time introduced the nano-fluid which is a revolutionary change in thermal transport and solved entropy problem in heat management systems. Nano-fluids are made by mixing nano-sized particles, ranging from 1 to 100 nm, of metals, oxides, or carbides in base fluids like water, carosene oil, *etc.* Nano-particles when added in fluid enhance thermal conductivity and surface area of thermal conduction, consequently enhancing the heat transfer rate. Nano-fluids are best coolants in heat transfer systems like heat exchangers, electronic cooling, and radiators. Polymerase chain reactions are efficiently enhanced by using graphene-based nano-fluids. In cold region, nano-fluids are used to heat the rooms more efficiently. By using nano-fluids, one can minimize the cost, loss of energy, and also the pollution. Kulkarni *et al.* [18] explored the application of nano-fluids in heating buildings and reducing pollution. Ramezanizadeh *et al.* [19] discussed in detail the application of nano-fluids in thermosiphons. Ebrahimnia-Bajestan *et al.* [20] worked on solar system heat exchanger with nano-fluids application. Li *et al.* [21] disclosed that the nano-fluids are best lubricants. Hamid [22] investigated the shape effects of nanoparticles on rotating flow of nano-fluids. A lot of contribution in this context can be found in refs [23–26].

The role of mathematical models in describing the different physical phenomena of daily life is more important. These models are composed of differential equations and some initial and boundary conditions. These differential equations are of different orders, may be integer order or non-integer fractional derivatives. But non-integer fractional derivatives have a vibrant scope in modern industrial era, as fractional models are more close to the geometry of physical systems. Also, fractional parameter is part of a solution which elaborated the memory effect more briefly helping to control the flow regime, consequently fractional models are considered superior than ordinary models. It was used to establish the models of the physical systems and many engineering processes by fractional differential equations. These models were found to be more accurately describing these fractional differential equations. Many physical phenomena of thermal transport, engineering, circuits, biotechnology, and signal process can be modified with the help of fractional derivative. Viscoelastic damping in polymers can be well modeled by using fractional derivative. Shape memory effect during deformation can be accurately described by using fractional calculus. Imran [27] explored the second grade fluid by using Caputo time fractional derivative analytically. Caputo and Fabrizio [28] presented a new fractional derivative having fruitful results of many physical problems. Ikram [29] investigated the flow of hybrid nano-fluid by using Caputo–Fabrizio (CF) derivative analytically. CF derivative involves non-singular kernel and it cannot produce original function when order of the derivative is zero. To overcome this problem, in 2016, Atangana and Baleanu [30] introduced new fractional derivative based on Mittag-Leffler function. Saqib *et al.* [31] investigated MHD channel flow of carbon nanotube-based nano-fluids by using ABC derivative. Wang [32] discussed heat and mass

transfer of Oldroyd-B nano-fluid by using ABC derivative *via* Laplace transform approach.

Viscous stresses destructing the fluctuating velocity gradient is known as viscous dissipation. Viscous dissipation effect is an irreversible process, which heats up the fluid because the viscosity of fluid takes energy from the motion of fluid and transforms it into internal energy of the fluid. Fruitful results with application of viscous dissipation, radiation, and magnetic field on nano-fluid are studied in refs [33,34]. Also, this effect was considered by Brinkman. Hussain *et al.* [35] explored the viscous dissipation effect in detail. Farooq [36] investigated the effect of viscous dissipation on entropy. Entropy is actually disordering or randomness of system. A loss of useful energy is known as entropy. Habib [37] discussed the entropy generation and heat transfer in power law fluid flow. Khan *et al.* [38] explored the entropy generation in nano-fluid flow between two rotating discs.

By following through literature discussed earlier, it is worth remarking that MHD Oldroyd-B nano-fluid model with thermal radiation, viscous dissipation, and heat source/sink in view of Caputo time fractional derivative is not considered and solved numerically *via* finite difference method (FDM). Furthermore, entropy generation, Bejan number, Nusselt number, and skin friction are calculated for the proposed model and compared with the existing literature.

2 Mathematical formulations

Let us consider the unsteady natural convection flow of incompressible fractional Oldroyd-B nano-fluid over infinite oscillating vertical plate as $\boldsymbol{V} = u_0 H(t)\mathrm{Cos}(\omega t)i$, where $H(t)$ is the unit step function, i is the unit vector in vertical flow direction, and ω is the frequency of oscillating plate. The plate is situated at $y = 0$, parallel to x-axis and moving in x-direction. Initially, both the plate and fluid are at rest with constant temperature θ_∞. For $t > 0$, the plate started oscillating motion with velocity $u_0\mathrm{H}(t)\cos(wt)$ and the temperature of plate raised by θ_w. Magnetic field is applied parallel to y-axis. Taking viscous dissipation as significant, velocity profile is of the form $\boldsymbol{V}(u(y, t), 0,0)$ as shown in Figure 1. The proposed model contains the following assumptions.

- Flow is unsteady, incompressible, and unidirection
- Pressure gradient is neglected
- Applying magnetic field (neglecting induced magnetic field)
- Considering thermal radiation along y-direction
- Viscous dissipation is significant.

Under the above described assumptions, momentum and energy equation are given as,

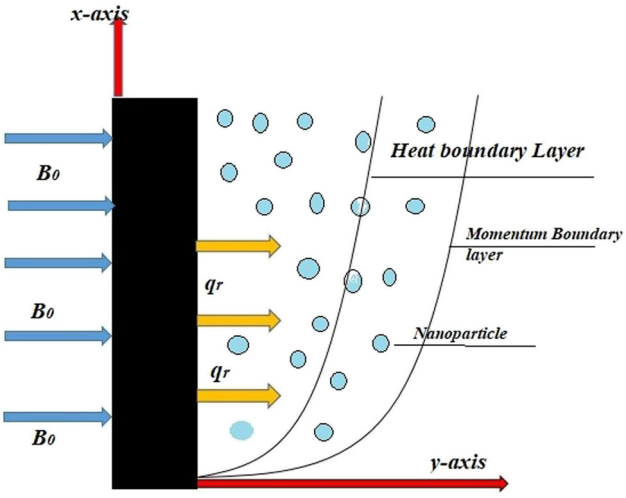

Figure 1: Geometry of flow dynamics.

The basic governing equations of the problem are given [40] as,

$$\nabla.\ \mathbf{V} = 0, \rho\left[\frac{\partial V}{\partial t} + (\mathbf{V}.\ \nabla)\mathbf{V}\right] = \rho g + J \times M + \mathrm{div}(\mathbf{T}), \quad (1)$$

where $\boldsymbol{V}$ is the velocity vector, M is the magnetic field parameter, $\boldsymbol{\rho}$ is the fluid density, the current density is represented by J, $\mathbf{T}$ is the Cauchy stress tensor, and t is the time and ρg is the other body forces. In case of Oldroyd-B nano-fluid, the relation between the extra stress tensor and Cauchy stress tensor is given [40] as,

$$T = -pI + S, \quad (2)$$

where

$$S + \lambda_1 \frac{\mathrm{D}S}{\mathrm{D}t} = \mu\left(A_1 + \lambda_2 \frac{\mathrm{D}A_1}{\mathrm{D}t}\right), \quad (3)$$

and

$$\frac{\mathrm{D}S}{\mathrm{D}t} = \frac{\mathrm{d}S}{\mathrm{d}t} - LS - SL^t, \frac{\mathrm{D}A_1}{\mathrm{D}t} = \frac{\mathrm{d}A_1}{\mathrm{d}t} - LA_1 - A_1L^t, \quad A_1 = L + L^t, L = \nabla V, \quad (4)$$

where ρ is the density, T is the Cauchy stress tensor, p is the pressure, I is the identity matrix, b is the body force, S is the extra stress tensor, $A_1$is the first Rivilin-Erikson tensor, λ_1 and λ_2 are the time relaxation parameters, λ_r is the time retardation parameter, and L is the velocity gradient.

By using Eqs. (2)–(4) in Eq. (1),

$$\rho_{hnf}\left(\frac{\partial u}{\partial t}\right) = \frac{\partial S_{xy}}{\partial y} + g(\rho\beta_\theta)_{nf}(\theta - \theta_\infty) - (\sigma)_{nf}B_0^2 u, \quad (5)$$

where S_{xy} is the extra stress tensor, β_θ is the coefficient of thermal expansion,σ is the electrical conductivity, B_o is

the applied magnetic field, and θ is the temperature. Multiplying Eq. (5) by $(1 + \lambda_1^{\alpha} D_t^{\alpha})$

$$\begin{aligned}\rho_{nf}(1 + \lambda_1^{\alpha} D_t^{\alpha})\left(\frac{\partial u}{\partial t}\right) &= \frac{\partial}{\partial y}(1 + \lambda_1^{\alpha} D_t^{\alpha}) S_{xy} \\ &+ g(\rho\beta_\theta)_{nf}(1 + \lambda_1^{\alpha} D_t^{\alpha})(\theta - \theta_\infty) \\ &- (\sigma)_{nf} B_0^2 (1 + \lambda_1^{\alpha} D_t^{\alpha}) u,\end{aligned} \tag{6}$$

The constitutive relation for Oldroyd-B fluid is given [40] as,

$$(1 + \lambda_1^{\alpha} D_t^{\alpha}) S_{xy} = \mu_{nf}(1 + \lambda_r^{\alpha} D_t^{\alpha}) \frac{\partial u}{\partial y}. \tag{7}$$

Applying Eq. (7) in Eq. (6)

$$\begin{aligned}(1 + \lambda_1^{\alpha} D_t^{\alpha}) \rho_{nf} \frac{\partial u}{\partial t} &= (1 + \lambda_r^{\alpha} D_t^{\alpha}) \mu_{nf} \frac{\partial^2 u}{\partial y^2} \\ &+ (1 + \lambda_1^{\alpha} D_t^{\alpha}) g(\rho\beta_\theta)_{nf}(\theta - \theta_\infty) \\ &- (1 + \lambda_1^{\alpha} D_t^{\alpha}) \sigma_{nf} B_0^2 u.\end{aligned} \tag{8}$$

Energy equation in the presence of thermal radiations and heat source/sink with viscous dissipation effect is given [41] as,

$$\begin{aligned}(\rho C_p)_{nf}\left(\frac{\partial \theta}{\partial t}\right) &= K_{nf} \frac{\partial^2 \theta}{\partial y^2} - \frac{\partial q_r}{\partial y} + \mu_{nf}\left(\frac{\partial u}{\partial y}\right)^2 \\ &+ Q(\theta - \theta_\infty),\end{aligned} \tag{9}$$

where $(C_p)_{nf}$ is the specific heat capacity of nanofluid at constant pressure, $(\rho)_{nf}$ is the density of nano-fluid, K_{nf} is the thermal conductivity of nano-fluid,$\mu_{nf}$is the dynamic viscosity of nano-fluid, q_r is the radiative heat flux, and Q is the heat source/sink parameter.

Under the Rosseland's approximation in ref. [32], q_r takes the following form

$$q_r = \left(\frac{-4\sigma^*}{3k^*}\right) \frac{\partial \theta^4}{\partial y}, \tag{10}$$

where σ^* is the Stefan–Boltzmann constant and k^* is the absorption constant. Expanding θ^4 about θ_∞ by using Taylor series

$$\theta^4 = 4\theta_\infty^3 \theta' - \theta_\infty^4. \tag{11}$$

Neglecting higher power of θ and using Eqs. (10) and (11) in Eq. (9), also multiplying with $(1 + \lambda_2^{\beta} D_t^{\beta})$, Eq. (9) takes the following form

$$\begin{aligned}&(\rho C_p)_{nf}(1 + \lambda_2^{\beta} D_t^{\beta})\left(\frac{\partial \theta}{\partial t}\right) \\ &= K_{nf}(1 + \lambda_2^{\beta} D_t^{\beta}) \frac{\partial^2 \theta}{\partial y^2} + \frac{16\sigma^* \theta_\infty^3}{3k^*}(1 + \lambda_2^{\beta} D_t^{\beta}) \frac{\partial^2 \theta}{\partial y^2} \\ &+ (1 + \lambda_2^{\beta} D_t^{\beta}) \mu_{nf}\left(\frac{\partial u}{\partial y}\right)^2 + (1 + \lambda_2^{\beta} D_t^{\beta}) Q(\theta - \theta_\infty).\end{aligned} \tag{12}$$

Associated initial and boundary conditions [42] are,

$$u(y, 0) = 0, u(0, t) = u_o H(t)\cos(\mathrm{wt}), u(\infty, t) = 0, \tag{13}$$

$$\theta(y, 0) = \theta_\infty, \theta(0, t) = \theta_w, \theta(\infty, t) = \theta_\infty. \tag{14}$$

For the proposed model, following are the non-dimensional quantities [42]

$$\begin{aligned}&u^* = \frac{u}{u_0}, t^* = \frac{u_0^2}{\nu} t, \theta^* = \frac{\theta - \theta_\infty}{\theta_w - \theta_\infty}, \lambda_1^* = \frac{u_0^2}{\nu}\lambda_1, \\ &\lambda_2^* = \frac{u_0^2}{\nu}\lambda_2, y^* = \frac{u_0 y}{\nu},\end{aligned}$$

Using these transformations in Eqs. (9) and (12–14)

$$\begin{aligned}&\mathrm{Gr} = \frac{\nu g(\beta_\theta)_f(\theta_w - \theta_\infty)}{u_0^3}, H_a^2 = M = \frac{\sigma_f B_0^2 \nu}{\rho_f u_0^{\,2}}, \\ &\mathrm{Pr} = \frac{\mu(C_p)_f}{K_f}, \mathrm{Nr} = \frac{16\sigma^* \theta_\infty^3}{a_5 3k^* K_f}, \\ &\mathrm{Ec} = \frac{\mu_f}{k_f}\left(\frac{u_0^2}{\nu(\theta_w - \theta_\infty)}\right), Q_0 = \frac{Q\nu}{a_5 K_f u_0^{\,2}}.\end{aligned} \tag{15}$$

where relation for nano-fluids are given [43] as

$$\left.\begin{aligned}&\frac{\rho_{nf}}{\rho_f} = a_1 = \left[(1 - \phi) + \phi\frac{\rho_s}{\rho_f}\right], \\ &\frac{(\rho\beta_\theta)_{nf}}{(\rho\beta_\theta)_f} = a_2 = \left[(1 - \phi) + \phi\left(\frac{(\rho\beta_\theta)_s}{(\rho\beta_\theta)_f}\right),\right] \\ &\frac{\mu_{nf}}{\mu_f} = a_3 = \left[\frac{1}{(1 - \phi)^{2.5}}\right], \\ &\frac{(\rho C_p)_{nf}}{(\rho C_p)_f} = a_4 = \left[(1 - \phi) + \phi\left(\frac{(\rho C_p)_s}{(\rho C_p)_f}\right)\right], \\ &\frac{k_{nf}}{k_f} = a_5 = \left[\frac{(k_s + 2k_f) - 2\phi(k_f - k_s)}{(k_s + 2k_f) + \phi(k_f - k_s)}\right], \\ &\frac{(\sigma)_{nf}}{(\sigma)_f} = a_6 = \left[1 + \frac{3\left(\frac{\sigma_s}{\sigma_f} - 1\right)\phi}{\left(\frac{\sigma_s}{\sigma_f} - 2\right) - \left(\frac{\sigma_s}{\sigma_f} - 1\right)\phi}\right]\end{aligned}\right\}, \tag{16}$$

$$b_1 = \frac{a_3}{a_1}, b_2\frac{a_2}{a_1}, b_3 = \frac{a_6}{a_1}, b_4 = \frac{a_4}{a_5}, b_5 = \frac{a_3}{a_5}, b_6 = \frac{a_6}{a_5}. \tag{17}$$

The dimensionless forms of the momentum and heat equations are

$$\begin{aligned}(1 + \lambda_1^{\alpha} D_t^{\alpha})\left(\frac{\partial u}{\partial t}\right) &= (1 + \lambda_r^{\alpha} D_t^{\alpha}) b_1 \left(\frac{\partial^2 u}{\partial y^2}\right) \\ &+ b_2 \mathrm{Gr}(1 + \lambda_1^{\alpha} D_t^{\alpha})(\theta) \\ &- b_3 H_a^2 (1 + \lambda_1^{\alpha} D_t^{\alpha})(u),\end{aligned} \tag{18}$$

$$\begin{aligned}b_4 \mathrm{Pr}(1 + \lambda_2^{\beta} D_t^{\beta})\left(\frac{\partial \theta}{\partial t}\right) &= (1 + \mathrm{Nr})(1 + \lambda_2^{\beta} D_t^{\beta}) \frac{\partial^2 \theta}{\partial y^2} \\ &+ b_5 \mathrm{Ec}(1 + \lambda_2^{\beta} D_t^{\beta})\left(\frac{\partial u}{\partial y}\right)^2 \\ &+ (1 + \lambda_2^{\beta} D_t^{\beta}) Q_0 \theta.\end{aligned} \tag{19}$$

Also, the dimensionless initial and boundary conditions

$$u(y, 0) = 0, u(0, t) = H(t)\cos(wt), u(\infty, t) = 0, \quad (20)$$

$$\theta(y, 0) = 0, \theta(0, t) = 1, \theta(\infty, t) = 0. \quad (21)$$

3 Entropy generation

For the Oldroyd-B fluid flow in magnetic field, the volumetric entropy generation of nano-fluid is given [44] as

$$E_G = E_\theta + E_f + E_m, \quad (22)$$

where E_θ, E_f, and E_m are entropy generated due to heat transfer, friction, and magnetic field effect, respectively. These terms are defined as,

$$E_\theta = \frac{K_{nf}}{\theta_\infty^2}\left(1 + \frac{16\sigma^\star\theta_\infty^3}{3k^\star K_{nf}}\right)\left(\frac{\partial\theta}{\partial y}\right)^2, E_f = \frac{\mu_{nf}}{\theta_\infty}\left(\frac{\partial u}{\partial y}\right)^2, \quad E_m = \frac{\sigma_{nf}B_0^2}{\theta_\infty}u^2. \quad (23)$$

By using Eq. (23) in Eq. (22)

$$\mathrm{Ns} = \frac{E_G}{E_0} = \left[a_5(1 + \mathrm{Nr})\left(\frac{\partial\theta}{\partial y}\right)^2 + a_3\frac{\mathrm{Br}}{\Omega}\left(\frac{\partial u^\star}{\partial y}\right)^2 + a_6\frac{\mathrm{Br}}{\Omega}H_a(u)^2\right]. \quad (24)$$

Here E_0 is the characteristic entropy generation rate, Br is the Brinkman number, H_a^2 is the Hartmann number, and Ω is dimensionless temperature difference given as

$$E_0 = \frac{K_f}{\nu_f^2}\frac{u_0^2(\theta_w - \theta_\infty)^2}{\theta_\infty^2}, \Omega = \frac{(\theta_w - \theta_\infty)}{\theta_\infty}, \quad \mathrm{Nr} = \frac{16\sigma^\star\theta_\infty^3}{3k^\star K_{nf}}, \mathrm{Br} = \frac{\mu_f u_0^2}{K_f(\theta_w - \theta_\infty)}, \text{ and } H_a^2 = \frac{\sigma_f B_0^2\nu}{\rho_f u_0^{\,2}}. \quad (25)$$

3.1 Bejan number

The Bejan number for the proposed model is defined [44] as

$$\mathrm{Be} = \frac{\frac{K_{nf}}{\theta_\infty^2}\left(\frac{\partial\theta}{\partial y}\right)^2}{\frac{K_{nf}}{\theta_\infty^2}\left(1 + \frac{16\sigma^\star\theta_\infty^3}{3k^\star K_{nf}}\right)\left(\frac{\partial\theta}{\partial y}\right)^2 + \frac{\mu_{nf}}{\theta_\infty}\left(\frac{\partial u}{\partial y}\right)^2 + \frac{\sigma_{nf}B_0^2}{T_\infty}u^2}, \quad (26)$$

$$\mathrm{Be} = \frac{\left(\frac{\partial\theta}{\partial y}\right)^2}{\left[(1 + \mathrm{Nr})\left(\frac{\partial\theta}{\partial y}\right)^2 + b_5\frac{\mathrm{Br}}{\Omega}\left(\frac{\partial u}{\partial y}\right)^2 + b_6\frac{\mathrm{Br}}{\Omega}H_a(u)^2\right]}. \quad (27)$$

3.2 Skin friction coefficient

Skin friction for the considered model is defined [45] as

$$C_f = -u_y(0, t). \quad (28)$$

3.3 Local Nusselt number

Nusselt number for the proposed model is calculated by the given definition [45] as

$$\mathrm{Nu} = -\theta_y(0, t). \quad (29)$$

4 Methodology

In this section, we proposed a finite difference scheme to handle the governing set of fractional-order fluid problem and heat transfer. For this, the discretization of the derivative of fractional-order of u, u_t, and u_{yy} are specified [46] as,

$${}_0^C D_{t_{j+1}}^\alpha u(y_i, t_{j+1}) = \frac{\Delta t^{-\alpha}}{\Gamma(2-\alpha)}[u_i^{j+1} - u_i^j] + \frac{\Delta t^{-\alpha}}{\Gamma(2-\alpha)}\sum_{l=1}^{j}(u_i^{j-l+1} - u_i^{j-l})d_l^\alpha, \quad (30)$$

$${}_0^C D_{t_{j+1}}^{1+\alpha} u(y_i, t_{j+1}) = \frac{\Delta t^{-(1+\alpha)}}{\Gamma(2-\alpha)}[u_i^{j+1} - 2u_i^j + u_i^{j-1}] + \frac{\Delta t^{-(1+\alpha)}}{\Gamma(2-\alpha)} \times \sum_{l=1}^{j}(u_i^{j-l+1} - 2u_i^{j-l} + u_i^{j-l-1})d_l^\alpha, \quad (31)$$

$$\frac{\partial}{\partial t}u(y_i, t_{j+1})\Big|_{t=t_{j+1}} = \frac{1}{\Delta t}[u_i^{j+1} - u_i^j], \quad (32)$$

$$\frac{\partial^2}{\partial y^2}u(y_{i+1}, t_j)\Big|_{y=y_{i+1}} = \frac{1}{\Delta y^2}[u_{i+1}^{j+1} - 2u_i^{j+1} + u_{i-1}^{j+1}]. \quad (33)$$

In the above expressions, $d_l^\alpha = -l^{1-\alpha} + (1 + l)^{1-\alpha}$ for $l = 1,2,3,\ldots, j$. Now, the rectilinear grid is assumed to examine the solution of the governing set of fractional-order fluid problem and heat transfer having grid spacing $\Delta y > 0, \Delta t > 0$ in the direction of space and time separately, where $\Delta t = \frac{T}{N}$, $\Delta x = \frac{L}{M}$ for Δy, Δt from $\mathbb{Z}^+$. The inner points (y_i, t_j) in the discussed domain $\Omega = [0, T] \times [0, L]$ are given as $i\Delta y = y_i$ and $j\Delta t = t_j$. The discretization of the governing set of fractional-order fluid problem and heat transfer at (y_i, t_j) is given as.

$$\frac{1}{\Delta t}(u_i^{j+1}-u_i^j)+\frac{\lambda_1^\alpha\Delta t^{-(1+\alpha)}}{\Gamma(2-\alpha)}(u_i^{j+1}-2u_i^j+u_i^{j-1})+\frac{\lambda_1^\alpha\Delta t^{-(1+\alpha)}}{\Gamma(2-\alpha)}$$
$$\times\sum_{l=1}^{j}(u_i^{j-l+1}-2u_i^{j-l}+u_i^{j-l-1})b_l^\alpha=\frac{b_1}{\Delta y^2}(u_{i+1}^{j+1}-2u_i^{j+1}+u_{i-1}^{j+1})$$
$$+\frac{b_1\lambda_2^\alpha\Delta t^{-\alpha}}{\Delta y^2\Gamma(2-\alpha)}\sum_{l=0}^{j}(u_{i+1}^{j-l+1}-2u_{i+1}^{j-l}+u_{i+1}^{j-l-1})b_l^\alpha-\frac{2b_1\lambda_2^\alpha\Delta t^{-\alpha}}{\Delta y^2\Gamma(2-\alpha)}$$
$$\times\sum_{l=0}^{j}(u_i^{j-l+1}-2u_i^{j-l}+u_i^{j-l-1})b_l^\alpha+\frac{\lambda_2^\alpha\Delta t^{-\alpha}}{\Delta y^2\Gamma(2-\alpha)}\sum_{l=0}^{j}(u_{i-1}^{j-l+1}-2u_{i-1}^{j-l}+u_{i-1}^{j-l-1})b_l^\alpha$$
$$+b_2\mathrm{Gr}\theta_i^{j+1}+\frac{c_2\mathrm{Gr}\Delta t^{-\alpha}}{\Gamma(2-\alpha)}(\theta_i^{j+1}-\theta_i^j)+\frac{b_2\mathrm{Gr}\Delta t^{-\alpha}}{\Gamma(2-\alpha)}\sum_{l=1}^{j}(\theta_i^{j-l+1}-\theta_i^{j-l})b_l^\alpha-b_3H_a^2u_i^{j+1}$$
$$-\frac{b_3H_a^2\Delta t^{-\alpha}}{\Gamma(2-\alpha)}(u_i^{j+1}-u_i^j)+\frac{b_3H_a^2\Delta t^{-\alpha}}{\Gamma(2-\alpha)}\sum_{l=1}^{j}(u_i^{j-l+1}-u_i^{j-l})b_l^\alpha,$$
$$\frac{b_4Pr}{\Delta t}(\theta_i^{j+1}-\theta_i^j)+\frac{b_4\mathrm{Pr}\lambda_2^\beta\Delta t^{-(1+\beta)}}{\Gamma(2-\beta)}(\theta_i^{j+1}-2\theta_i^j+\theta_i^{j-1})$$
$$+\frac{b_4\mathrm{Pr}\lambda_2^\beta\Delta t^{-(1+\beta)}}{\Gamma(2-\beta)}\sum_{l=1}^{j}(\theta_i^{j-l+1}-2\theta_i^{j-l}+\theta_i^{j-l-1})b_l^\beta=\frac{1+\mathrm{Nr}}{\Delta y^2}(\theta_{i+1}^{j+1}-2\theta_i^{j+1}+\theta_{i-1}^{j+1})$$
$$+\frac{(1+\mathrm{Nr})\lambda_2^\beta\Delta t^{-\beta}}{\Delta y^2\Gamma(2-\beta)}\sum_{l=0}^{j}(\theta_{i+1}^{j-l+1}-2\theta_{i+1}^{j-l}+\theta_{i+1}^{j-l-1})b_l^\beta-\frac{(1+\mathrm{Nr})2\lambda_2^\beta\Delta t^{-\beta}}{\Delta y^2\Gamma(2-\beta)}$$
$$\times\sum_{l=0}^{j}(\theta_i^{j-l+1}-2\theta_i^{j-l}+\theta_i^{j-l-1})b_l^\beta+\frac{(1+\mathrm{Nr})\lambda_2^\beta\Delta t^{-\beta}}{\Delta y^2\Gamma(2-\beta)}\sum_{l=0}^{j}(\theta_{i-1}^{j-l+1}-2\theta_{i-1}^{j-l}+\theta_{i-1}^{j-l-1})b_l^\beta$$
$$+\frac{b_5}{\Delta y^2}Ec(u_{i+1}^j-u_i^j)(u_{i+1}^{j+1}-u_i^{j+1})+\frac{b_5\lambda_2^\beta\Delta t^{-\beta}}{\Delta y^2\Gamma(2-\beta)}Ec(u_{i+1}^j-u_i^j)$$
$$\times\left(u_{i+1}^{j+1}-u_{i+1}^j-\sum_{l=1}^{j}(u_{i+1}^{j-l+1}-u_{i+1}^{j-l})b_l^\beta-u_i^{j+1}+u_i^j+\sum_{l=1}^{j}(u_i^{j-l+1}-u_i^{j-l})b_l^\beta\right)$$
$$+\frac{Q_0\Delta t^{-\beta}}{\Gamma(2-\beta)}(\theta_i^{j+1}-\theta_i^j)+\frac{Q_0\Delta t^{-\beta}}{\Gamma(2-\beta)}\sum_{l=1}^{j}(\theta_i^{j-l+1}-\theta_i^{j-l})b_l^\beta+Q_0\theta_i^{j+1}.$$

for $j=1,2,3,\ldots,N-1$, $i=1,2,3,\ldots,N-1$, with the following initial and boundary conditions,

$$u_i^0=0,\ u_i^1=u_i^{-1},\ \theta_i^0=0,\ \theta_i^1=\theta_i^{-1},\ \text{for } i=0,1,2,3,\ldots,M,$$
$$u_0^j=\cos(jw\Delta t),\ u_M^j=0,\ \theta_0^j=1,\ \theta_M^j=0,\ \text{for } j=1,2,3,\ldots,N-1.$$

Test Problem

In order to check the efficiency of the proposed algorithm, suppose the problem is

$${}_0^CD_t^\alpha U(x,t)=\frac{\partial^2}{\partial x^2}U(x,t)-\frac{\partial}{\partial x}U(x,t)+g(x,t).$$

Here the initial and boundary conditions are specified below and inhomogeneous term can be designated against the choice of fractional-order derivative.

$$U(x,0)=U(0,t)=U(L,t)=0.$$

The exact solution of the considered problem is $U(x,t)=x(x-t)t^2$. Several simulations have been accomplished to check the accuracy of the suggested method. Figure 2(a) and (b) are plotted between the various values of N and maximum absolute error (MAE), and the computational order of convergence (COC) given below,

$$\mathrm{MAE}=\max_{\substack{1\le i\le M\\1\le j\le N}}|U(x_i,t_j)-U_i^j|,\ \mathrm{COC}=\log\left(\frac{\mathrm{MAE}(k)}{\mathrm{MAE}(k+1)}\right)/\log\left(\frac{N(k+1)}{N(k)}\right).$$

It is well known that the method is convergent beside each fractional-order derivative and its convergence order increases as $\alpha\to1$. Figure 2(c) and (d) comprises the L_∞-norm among the consecutive solutions *i.e.*, $|U^{j+1}-U^j|_\infty$ and $|U_{i+1}-U_i|_\infty$ when $0\le i,j\le N$, $M=500$. It is established that the suggested method is very effective, reliable, and accurate for the considered problem. Solutions are unchanged against the fractional order mesh which validated the given solutions.

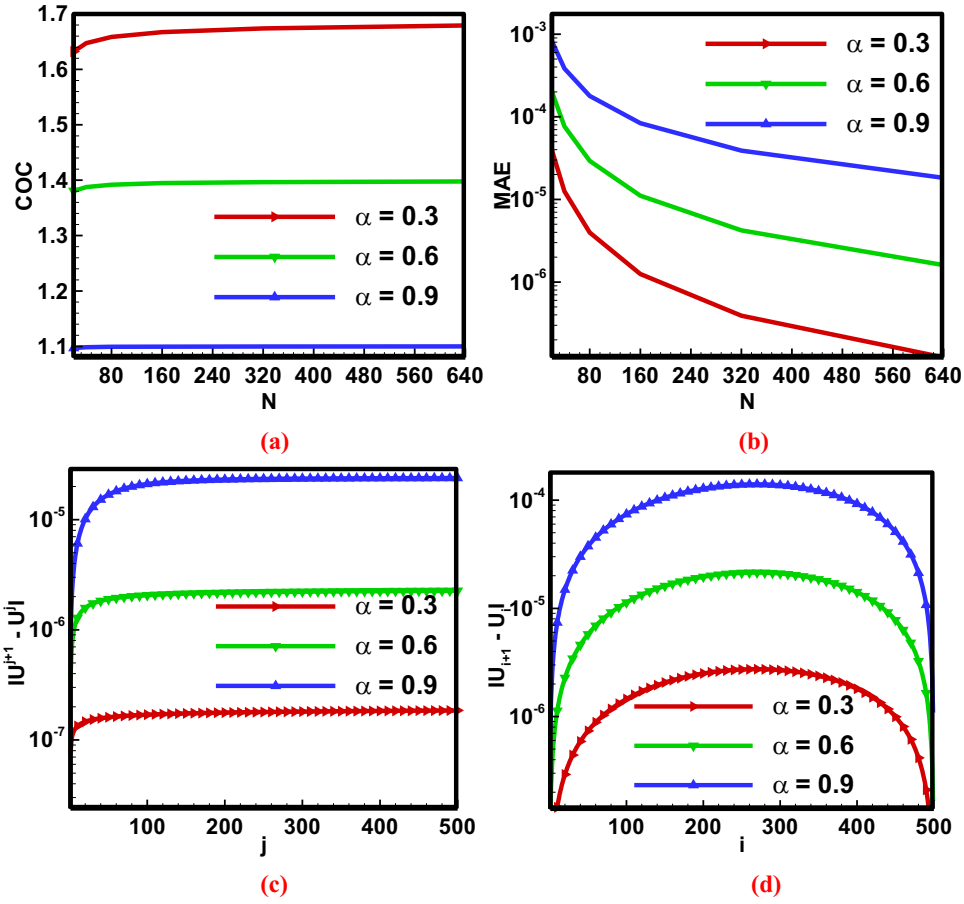

Figure 2: Code validation of the proposed scheme and varying time mesh size against (a) COC, (b) MAE, and varying mesh size for (c) time and (d) space against L_∞-norm between consective solutions.

5 Analysis and discussion of results

This section of the research work deals with the detailed overview of the key numerical findings and physical interpretation of different emerging parameters such as Gr, Pr, M, Ec, α, λ, Nr, Ns, Nu, C_f, ϕ, Q_0, and Be are the Grashof number, Prandtl number, magnetic field parameter, Eckert number, fractional parameter, time relaxation parameter, radiation parameter, entropy generation parameter, Nusselt number, skin friction, volume fraction parameter of nanoparticles, heat source/sink parameter, and Bejan number, respectively. The behavior of the velocity profile $u(y, t)$, temperature profile $\theta(y, t)$, and the effects of the mentioned physical parameters are deliberated as well as graphical illustration is made *via* MAPLE. The velocity profile, temperature profile, skin friction, Nusselt number, Bejan number, and entropy generation are calculated by assuming the different ranges $(0 \le Gr \le 5)$, $(0 \le Ha \le 5)$, $(3.94 \le Pr \le 15)$, $(0 \le Ec \le 5)$, $(0.2 \le \alpha, \beta \le 1)$, $(0.1 \le \lambda_1, \lambda_2 \le 0.5)$, $(0 \le Nr \le 5)$, $(0.1 \le \phi \le 0.2)$, and $(0 \le Q_0 \le 5)$. Discretization of time and spatial derivative is done using FDMs. The coupled, nonlinear, and fractional models have been solved numerically by using FDM which is a dominant tool to deal such kinds of problems.

Table 1: Thermo-physical properties of different materials taken from ref. [39]

Materials	ρ (kgm^{-3})	C_p (J Kg^{-1} k^{-1})	k (Wm^{-1} k^{-1})	$\beta \times 10^{-5}$ (k^{-1})	σ (Ωm)$^{-1}$
water	997	4,197	0.613	21	0.05
Cu (ϕ)	8,933	385	401	1.67	5.96×10^7

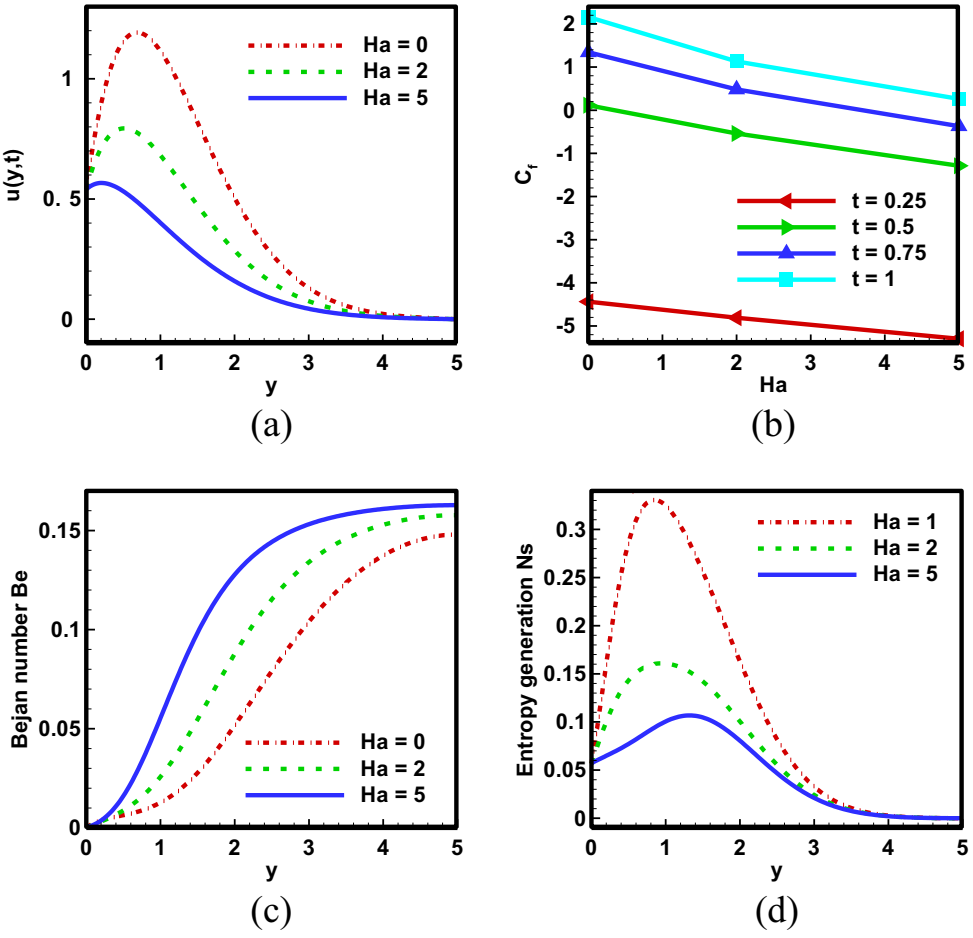

Figure 3: Impact of Hartmann number on (a) dimensionless velocity profile, (b) coefficient of skin friction, (c) Bejan number, and (d) entropy generation, when, $\alpha = \beta = 0.6$, $\Lambda_1 = 0.1$, $\Lambda_2 = 0.2$, Gr = 5, Pr = 6.2, $Q_0 = 2.5$, Nr = 5, Ec = 2, Br = 2, $\Omega = 10$, and $\phi = 0.1$.

Results are obtained by solving Eqs. (18) and (19) with initial and boundary conditions illustrated in Eqs. (20) and (21), and physical properties of nanoparticle in Eq. (16) and Table 1.

Figure 3a depicts the effect of magnetic field on fluid velocity. Enhancement in the strength of magnetic field parameter (Ha), causes a decrease in the fluid velocity. It can be justified as, by enhancing the magnetic field strength, actually the Lorentz force increased which shows a high resistance to fluid flow. Enhancing the magnetic field parameter amounts to stronger Lorentz force and hence rate of heat transfer in the boundary layer is higher. Bejan number (Be) is the ratio of entropy generation due to heat transfer to total entropy generation. By increasing the amount of magnetic field parameter there is an increase in Be as shown in Figure 3c. It means increase in Be by increasing the values of H_a^2 is due to the decrease in the total entropy generation as shown in Figure 3d. From Figure 3b, it can be seen that higher values of (Ha) maximizes the skin friction (C_f). Similar results are reported by Sarojamma *et al.* [47].

Figure 4a elaborates the effect of Grashof number Gr on the fluid velocity profile. Grashof number is the ratio of thermal buoyancy forces to the viscous forces. Fluid velocity increases by increasing the value of Gr as thermal buoyancy forces dominated the viscous force. There is an increase in C_f by enhancing the Gr as shown in Figure 4b. Higher values of Gr lowers the Be as shown in Figure 4c and higher entropy generation can be noticed in Figure 4d. These results are also reported in ref. [47].

Effect of Λ_1 on the fluid velocity is elaborated in Figure 5a. It can be seen that the enhancement in Λ_1 causes an increase in the fluid velocity. Skin friction

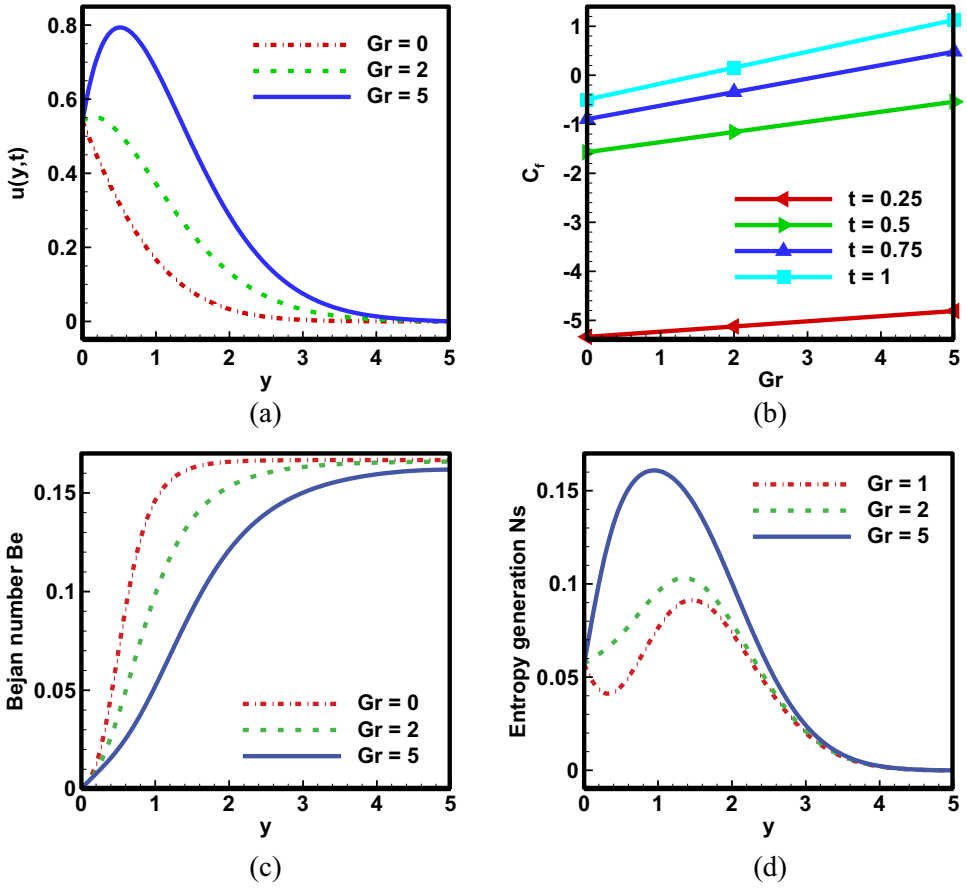

Figure 4: Influence of Grashof number on (a) dimensionless velocity profile, (b) coefficient of skin friction, (c) Bejan number, and (d) entropy generation, when $\alpha = \beta = 0.6$, $\Lambda_1 = 0.1$, $\Lambda_2 = 0.2$, Ha = 2, Pr = 6.2, $Q_0 = 2.5$, Nr = 5, Ec = 2, Br = 2, $\Omega = 10$, and $\phi = 0.1$.

increases by increasing Λ_1 as shown in Figure 5b. Be slightly increases by an increase in Λ_1 as shown in Figure 5c, and Ns decreased by increasing Λ_1, Figure 5d.

Effect of ϕ of nanoparticles on the fluid velocity profile is depicted in Figure 6a. Advancement in control of ϕ reduced the fluid velocity due to the fact that by increasing ϕ fluid becomes more viscous. Since the addition of nanoparticles increase the viscosity, consequently the velocity profile decreased. By increasing ϕ, heat transfer from boundary layer becomes better due to the enhanced thermal conductivity of the base fluid caused by nanoparticles which results in increasing the internal fluid temperature as shown in Figure 6b. There is a decrease in Nu by increasing ϕ as seen in Figure 6f. Effects of ϕ on (C_f) is elaborated in Figure 6e, by increasing the values of ϕ causes decrease in C_f. Heat transfer rate becomes good by increasing the ϕ and hence the values of (Be) are enhanced as seen in Figure 6c. Figure 6d depicts the effect of ϕ on entropy generation. Entropy enhanced by advancement in the values of ϕ because viscosity of the fluid increased by increasing ϕ. These results are also reported in ref. [48].

Figure 7a illustrates the behavior of fluid velocity against different values of fractional parameter ($\alpha = \beta$). By increasing the values of $\alpha = \beta$, thermal and momentum boundary layers are reduced and become thinnest for $\alpha = \beta = 1$, consequently increasing the fluid velocity, and decreasing the temperature as shown in Figure 7b. There is an increase in Be and Ns by enhancing the values of $\alpha = \beta$ as shown in Figure 7c and d, respectively.

Effects of Pr on fluid temperature are presented in Figure 8a. Increasing the values of Pr increased the

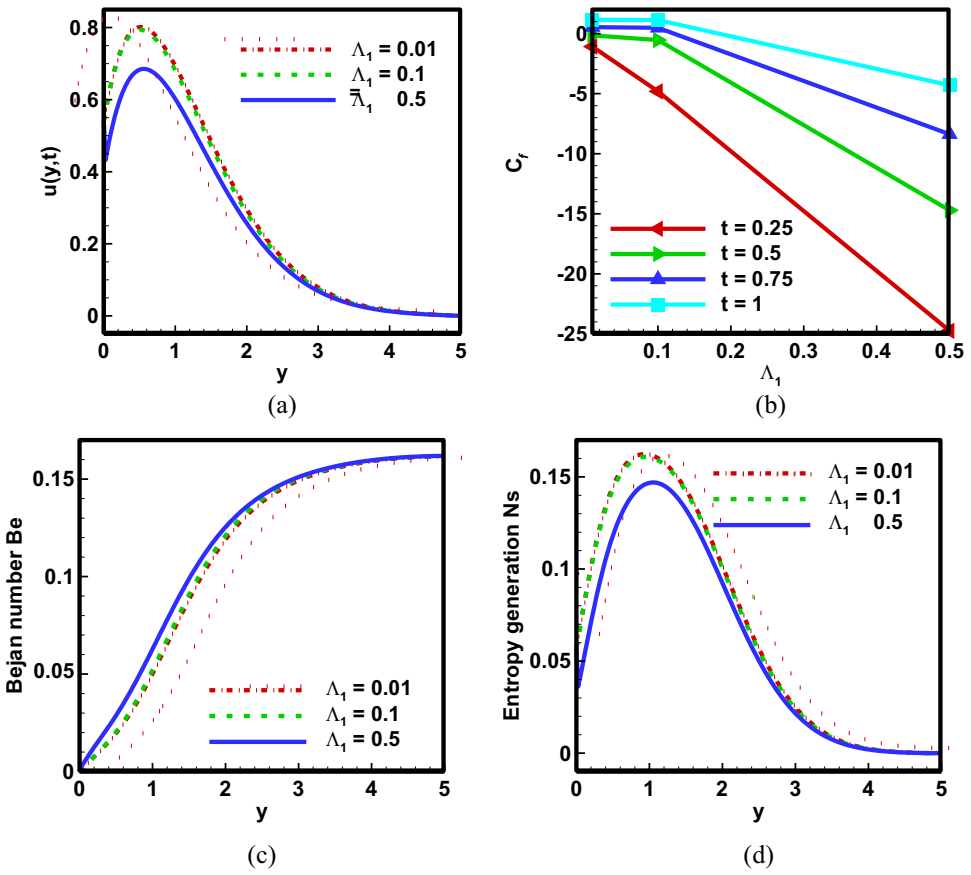

Figure 5: Effect of time relaxation parameter on (a) dimensionless velocity profile, (b) coefficient of skin friction, (c) Bejan number, and (d) entropy generation, when $\alpha = \beta = 0.6$, $\Lambda_1 = 0.1$, $\Lambda_2 = 0.2$, Gr = 5, Ha = 2, Pr = 6.2, $Q_0 = 2.5$, Nr = 5, Ec = 2, Br = 2, $\Omega = 10$, and $\phi = 0.1$.

viscous diffusion rate and decreased the thermal diffusion rate consequently, decreasing the fluid temperature. Pr reduced the values of Nu for enhancing the time parameter as can be seen in Figure 8b. It can be noticed from Figure 8c and d, respectively, that increasing the value of Pr decreased Be and Ns. Similar results are published in ref. [48].

Effects of Nr on temperature profile is elaborated in Figure 9a. Enhancement in Nr enhanced the fluid temperature, and reduced Nu for increasing time parameter in Figure 9b. It is a well-known fact that heat transfer plays a prominent role in the thermodynamic irreversibility. As Nr increased, it is noticed that Ns also increased in as shown in Figure 9c. Relative effect of heat transfer entropy generation and total entropy generation is measured by Be. It is observed that Be decreased near the surface of plate, and a little away from the surface, Be increased for increasing values of Nr. It can be justified as fluid friction reversibility is prominent near the surface, and at a distance from the surface, heat transfer irreversibility becomes prominent. Similar results are reported in ref. [47].

Relative effect of kinetic energy of flow on the enthalpy difference across the thermal boundary layer is measured by Ec. Increase in the value of Ec means decreasing the viscous dissipation and consequently increasing the fluid temperature as shown in Figure 10a. It is also noticed in Figure 10b that Nu decreased on increasing the values of time parameter against Ec. A slight increase in Be against increasing values of Ec is noticed in Figure 10c. Figure 10d presents the effect of Ec on Ns, it can be noticed that for increasing values of Ec, the entropy generation also increased.

Figure 11a illustrates the effect of time relaxation parameter ($\lambda_2 = \Lambda_2$) on fluid temperature. Advancement in Λ_2 causes decrease in fluid temperature. In Figure 11b,

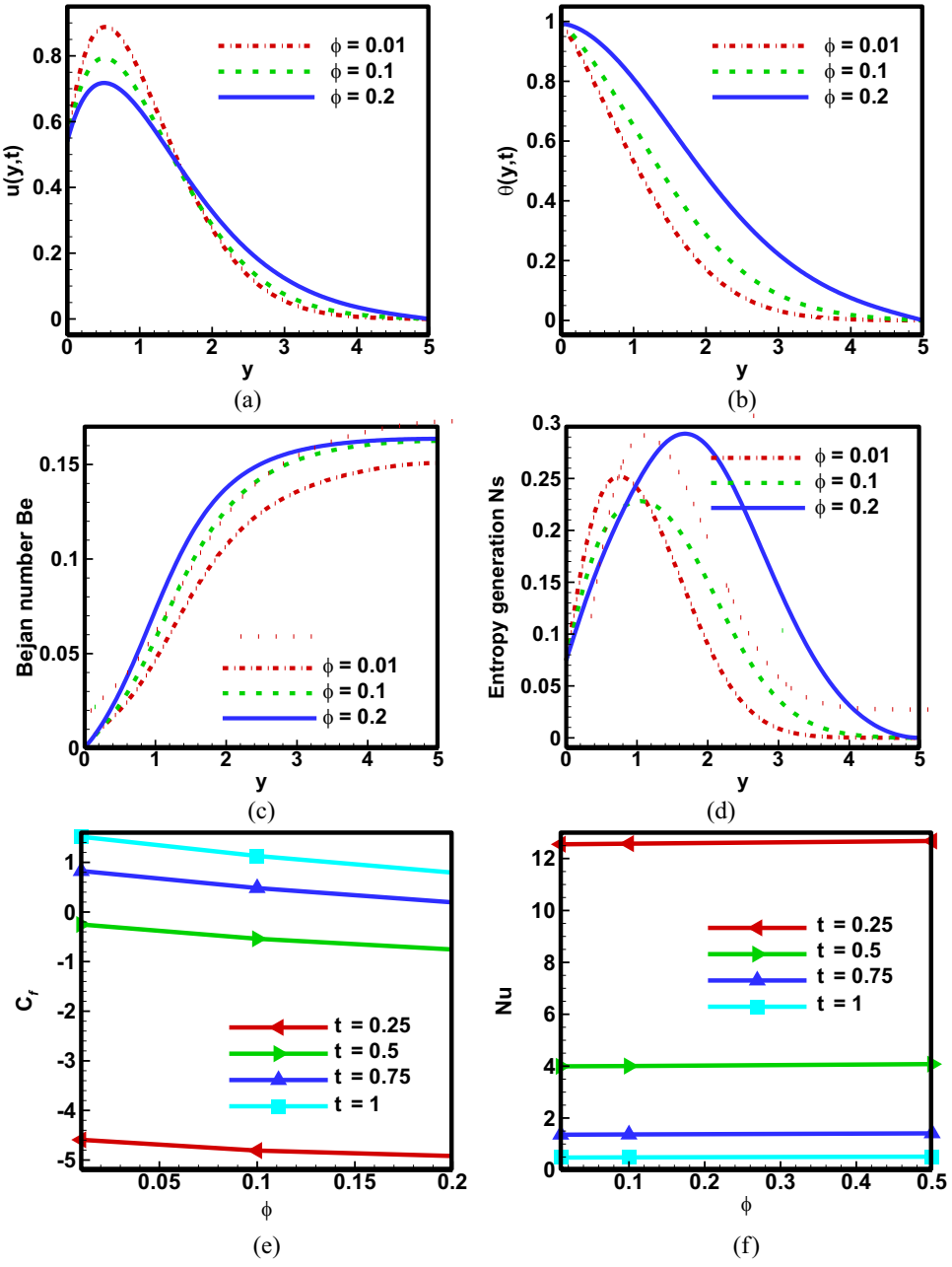

Figure 6: Effect of ϕ on (a) dimensionless velocity profile, (b) dimensionless temperature profile, (c) Bejan number, (d) entropy generation, (e) skin friction, and (f) Nusselt number, when $\alpha = \beta = 0.6$, $\Lambda_1 = 0.1$, $\Lambda_2 = 0.2$, Gr = 5, Ha = 2, Pr = 6.2, $Q_0 = 2.5$, Nr = 5, Ec = 2, Br = 2, and $\Omega = 10$.

it is examined that for higher values of time parameter against Λ_2, the values of Nu are reduced. Be and Ns have opposite behavior against Λ_2, as can be noticed that for enhancing values of Λ_2, the Be is also enhanced as shown in Figure 11c, but Ns decreased in as shown in Figure 11d.

Figure 12a depicts the effects of Q_0 on fluid temperature. Fluid temperature enhanced for advancement in the values of Q_0. Nu decreased for increasing values of Q_0 as can be noticed from Figure 12b. Be and Ns also increased for increasing values of Q_0. Similar results can be found in ref. [47], showing that present results have good agreement with the published results.

Tables 2 and 3 show the behavior of physical quantities, *i.e.*, skin friction coefficient and local Nusselt number on varying the physical parameters under discussion.

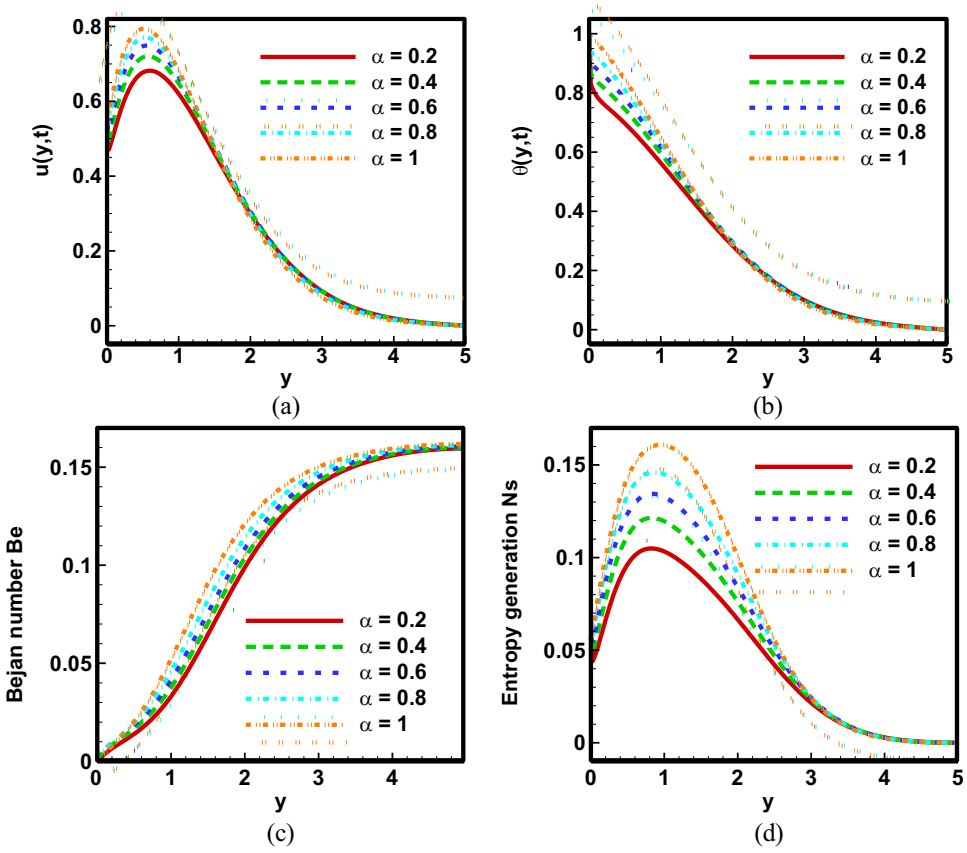

Figure 7: Impact of $\alpha = \beta$ on (a) dimensionless velocity profile, (b) dimensionless temperature profile, (c) Bejan number, and (d) entropy generation when $\Lambda_1 = 0.1$, $\Lambda_2 = 0.2$, Gr = 5, Ha = 2, Pr = 6.2, $Q_0 = 2.5$, Nr = 5, Ec = 2, Br = 2, $\Omega = 10$, and $\phi = 0.1$.

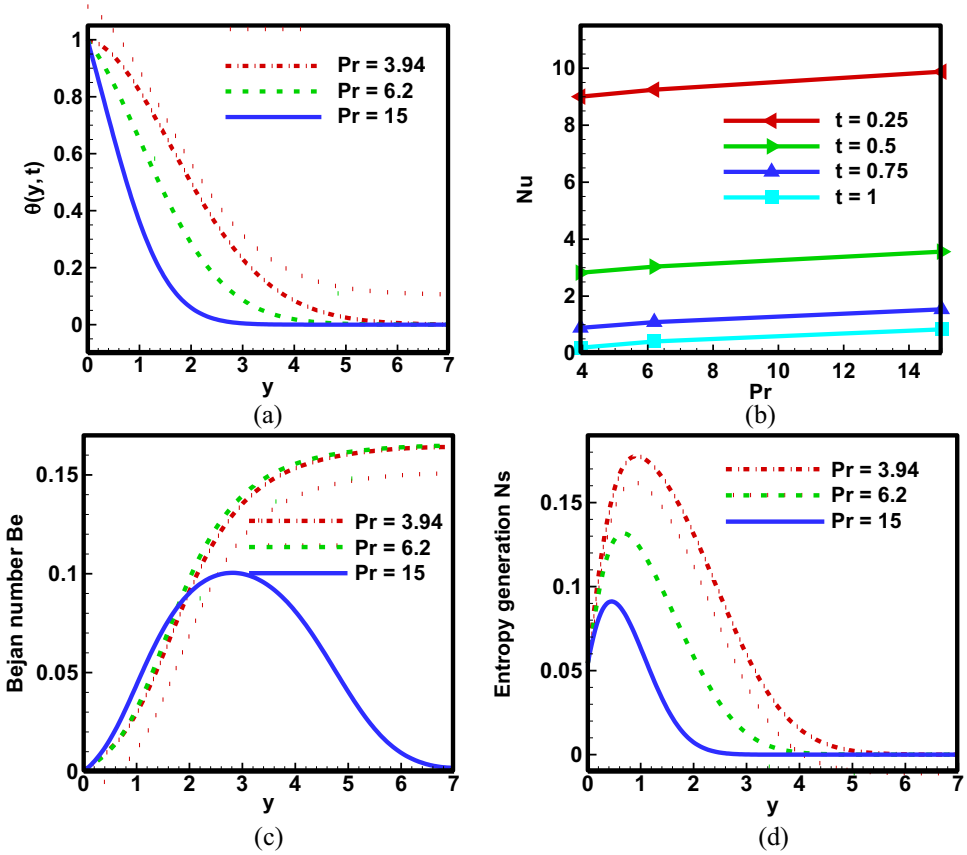

Figure 8: Effect of Pr on (a) dimensionless temperature profile, (b) Nusslt number, (c) Bejan number, and (d) entropy generation, when $\alpha = \beta = 0.6$, $\Lambda_1 = 0.1$, $\Lambda_2 = 0.2$, Gr = 5, Ha = 2, $Q_0 = 2.5$, Nr = 5, Ec = 2, Br = 2, $\Omega = 10$, and $\phi = 0.1$.

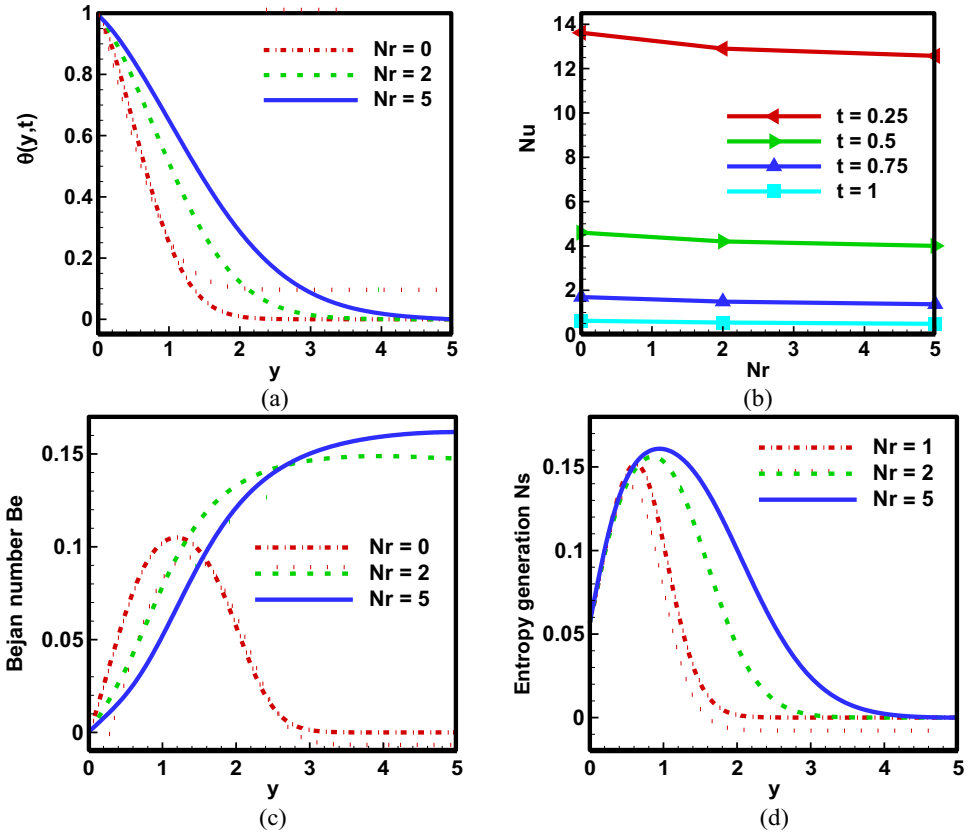

Figure 9: Effect of thermal radiations parameter (Nr) on (a) dimensionless temperature profile, (b) Nusslt number, (c) Bejan number, and (d) entropy generation, when $\alpha = \beta = 0.6$, $\Lambda_1 = 0.1$, $\Lambda_2 = 0.2$, Gr = 5, Ha = 2, Pr = 6.2, $Q_0 = 2.5$, Ec = 2, Br = 2, $\Omega = 10$, and $\phi = 0.1$.

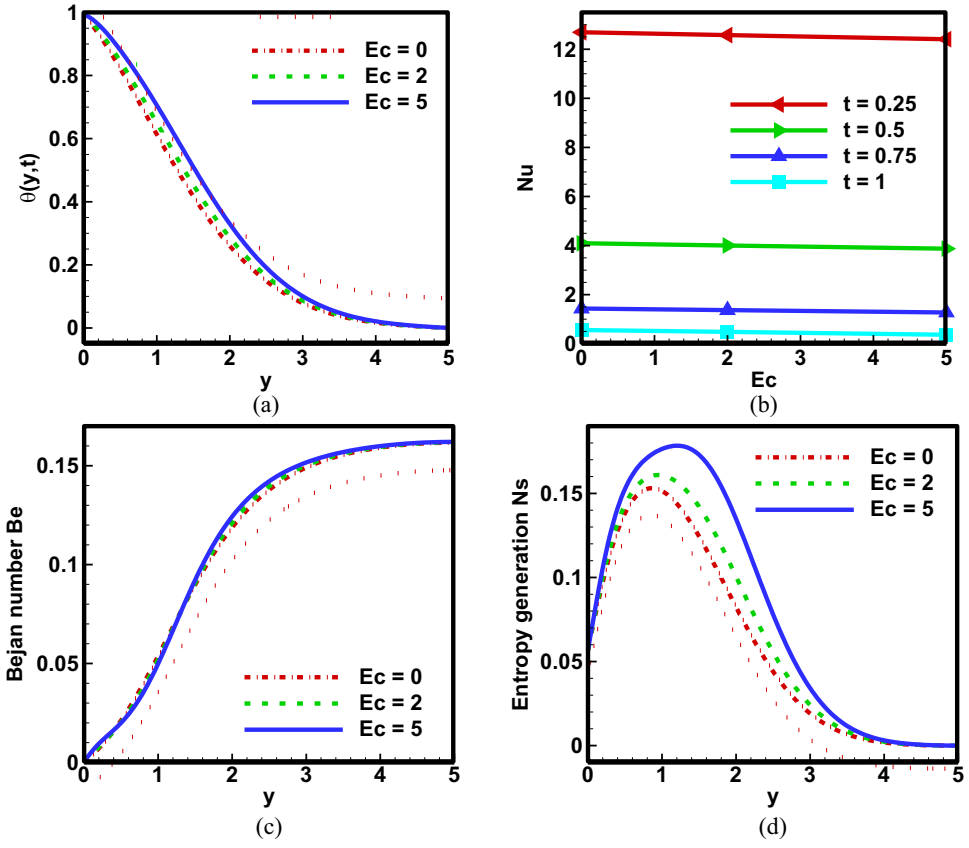

Figure 10: Effect of Ec on (a) dimensionless temperature profile, (b) Nusslt number, (c) Bejan number, and (d) entropy generation, when $\alpha = \beta = 0.6$, $\Lambda_1 = 0.1$, $\Lambda_2 = 0.2$, Gr = 5, Ha = 2, Pr = 6.2, $Q_0 = 2.5$, Nr = 5, Br = 2, $\Omega = 10$, and $\phi = 0.1$.

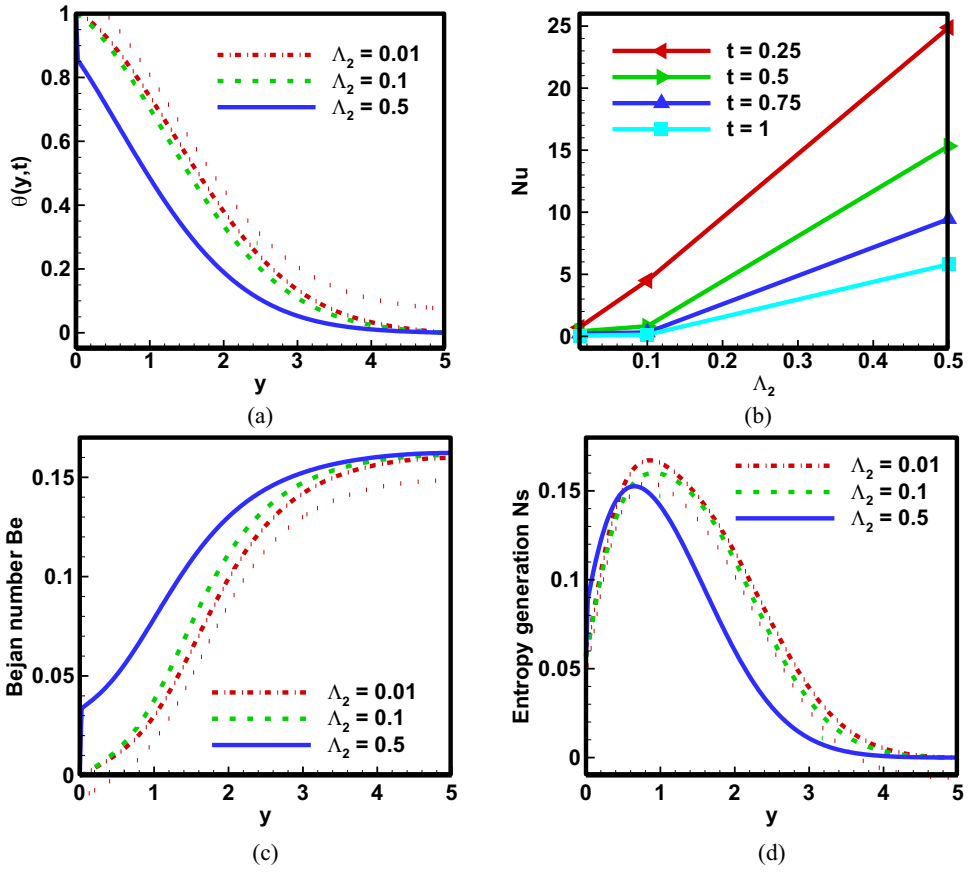

Figure 11: Effect of Λ_2 on (a) dimensionless temperature profile, (b) Nusslt number, (c) Bejan number, and (d) entropy generation, when $\alpha = \beta = 0.6$, $\Lambda_1 = 0.1$, Gr = 5, Ha = 2, Pr = 6.2, $Q_0 = 2.5$, Nr = 5, Ec = 2, Br = 2, $\Omega = 10$, and $\phi = 0.1$.

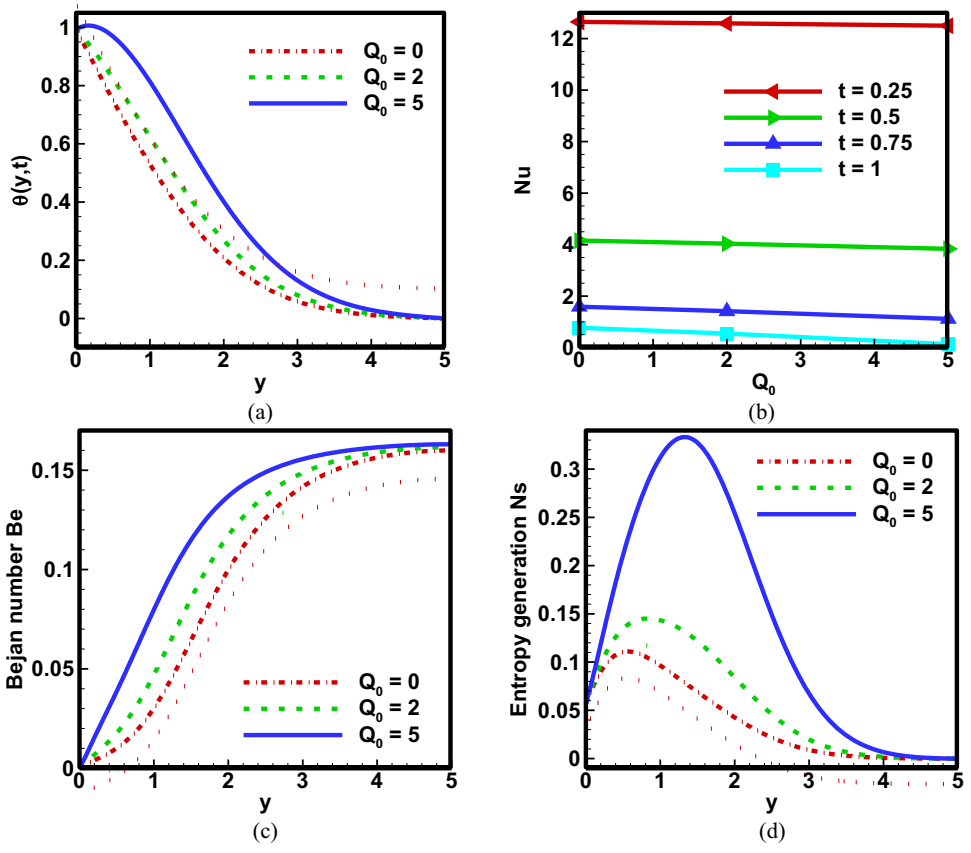

Figure 12: Effect of Q_0 on (a) dimensionless temperature profile, (b) Nusslt number, (c) Bejan number, and (d) entropy generation, when $\alpha = \beta = 0.6$, $\Lambda_1 = 0.1$, $\Lambda_2 = 0.2$, Gr = 5, Ha = 2, Pr = 6.2, Nr = 5, Ec = 2, Br = 2, $\Omega = 10$, and $\phi = 0.1$.

Table 2: Skin friction analysis against different physical parameters and $\alpha = \beta = v$

Ha	Gr	λ_1^{α}	$v = 0.4$	$v = 0.7$	$v = 1$
0.1	0.5	0.1	1.3535	0.6187	−0.1437
0.2			1.3854	0.6524	−0.1086
0.3			1.4163	0.6850	−0.7445
2.0	0.1	0.1	1.0966	1.2040	0.4722
	0.2		1.8841	1.1824	0.4495
	0.3		1.8636	1.1607	0.4268
2.0	0.5	0.1	1.8226	1.1174	0.3814
		0.2	3.0058	1.9186	0.5525
		0.3	4.0504	2.7811	1.1557

Table 3: Nusselt number analysis against different physical parameters and $\alpha = \beta = v$

Pr	Nr	Ec	$v = 0.4$	$v = 0.7$	$v = 1$
1	0.5	0.5	1.7262	1.0182	0.2809
2			1.7758	1.0685	0.3308
3			1.7951	1.0885	0.3512
6.2	0.1	0.5	3.5795	2.3869	0.9993
	0.2		3.5451	2.5582	0.9652
	0.3		3.5141	2.3281	0.9351
	0.5	0.1	3.5021	2.3271	0.9348
		0.2	3.4917	2.3155	0.9220
		0.3	3.4812	2.3040	0.9093

6 Conclusion

The fractional Oldroyd-B nano-fluid model in view of Caputo time fractional derivative along with infinite oscillating vertical plate has been investigated. The prevailing system of nonlinear partial differential equations is converted into dimensionless form. For the purpose of physical observations of the proposed model, a numerical scheme (FDM) is applied. Numerical solutions with parametric effects are elaborated by the mean of graphical figures portrayed using MAPLE. Key results are as follows:

- Reduction in the velocity profile of fluid flow is observed against change in Ha, λ_1, and ϕ.
- Temperature profile boosts for increasing values of Nr, ϕ, Q_0, and viscous dissipation parameter (Ec).
- Ns enhanced by enhancing the values of Gr, Ec, α, ϕ, Nr, and Q_0, and declined with the variation in Pr, Ha, λ_1, and λ_2.
- Be increased with the increase in the values of Ha, λ_1, λ_2, ϕ, α, and Q_0, and decreased for Gr and Pr. Dual nature for Nr and Ec) is noticed initially, *i.e.*, they decreased and then increased gradually.
- Nu decayed for the advancement in the values of Q_0, Nr, ϕ, λ_2, Ec, and Pr. And C_f boosts for increase in the values of Ha, Gr, ϕ, and λ_1.

The core contribution to literature is that enhancement occurs in temperature by enlarging the values of Ec, Nr, and Q_0. Ns is controlled by the addition of nanoparticles.

This problem can be extended for further effects like variable thermal conductivity and porous medium. Also, FDM is a very strong tool for solving such numerous type's problem and complex geometry.

Acknowledgments: The authors are thankful to the University of Management and Technology Lahore, 54770, Lahore Pakistan.

Funding information: The authors state no funding involved.

Author contributions: All authors have accepted responsibility for the entire content of this manuscript and approved its submission.

Conflict of interest: The authors state no conflict of interest.

References

[1] Ali A, Asjad MI. Numerical solutions of a heat transfer for fractional maxwell fluid flow with water based clay nanoparticles; A finite difference approach. Fractal Fract. 2021;5(4):242.
[2] Khan AS, Nie Y, Shah Z. Impact of thermal radiation on magnetohydrodynamic unsteady thin film flow of Sisko fluid over a stretching surface. Processes. 2019;7(6):369.
[3] Asjad MI. Heat transfer analysis of fractional second-grade fluid subject to Newtonian heating with Caputo and Caputo-Fabrizio fractional derivatives: A comparison. Eur Phys J Plus. 2017;132(8):1–19.
[4] Javaid M. Unsteady flow of fractional Burgers' fluid in a rotating annulus region with power law kernel. Alex Eng J. 2022;61(1):17–27.
[5] Aleem M, Asjad MI, Ahmadian A, Salimi M, Ferrara M. Heat transfer analysis of channel flow of MHD Jeffrey fluid subject to generalized boundary conditions. Eur Phys J Plus. 2020;135(1):1–15.
[6] Riaz MB, Imran M, Shabbir K. Analytic solutions of Oldroyd-B fluid with fractional derivatives in a circular duct that applies a constant couple. Alex Eng J. 2016;55(4):3267–75.
[7] Ali A, Hussain M, Anwar MS, Inc M. Mathematical modeling and parametric investigation of blood flow through a stenosis artery. Appl Math Mech. 2021;42(11):1675–84.
[8] Hussain Z. Mixed convective flow of CNTs nanofluid subject to varying viscosity and reactions. Sci Rep. 2021;11(1):1–14.
[9] Irfan M. Evaluating the performance of new mass flux theory on Carreau nanofluid using the thermal aspects of convective heat transport. Pramana. 2021;95(4):1–9.

[10] Rafiq K. Arrhenius activation energy theory in radiative flow of Maxwell nanofluid. Phys Scr. 2021;96(4):045002.
[11] Fetecau C, Prasad SC, Rajagopal KR. A note on the flow induced by a constantly accelerating plate in an Oldroyd-B fluid. Appl Math Model. 2007;31(4):647–54.
[12] Fetecau C, Hayat T, Khan M. Unsteady flow of an Oldroyd-B fluid induced by the impulsive motion of a plate between two side walls perpendicular to the plate. Acta mechanica. 2008;198(1):21–33.
[13] Gul T. Unsteady MHD thin film flow of an Oldroyd-B fluid over an oscillating inclined belt. PLoS one. 2015;10(7):e0126698.
[14] Wang J. Transportation of heat generation/absorption and radiative heat flux in homogeneous–heterogeneous catalytic reactions of non-Newtonian fluid (Oldroyd-B model). Comput methods Prog biomedicine. 2020;189:105310.
[15] Song YQ, Farooq A, Kamran M, Rehman S, Tamoor M, Khan R, et al. Analytical solution of fractional Oldroyd-B fluid *via* fluctuating duct. Complexity. 2021;2021:16.
[16] Hayat T. Cattaneo-Christov (CC) heat flux model for nanomaterial stagnation point flow of Oldroyd-B fluid. Comput Methods Prog Biomedicine. 2020;187:105247.
[17] Choi SU, Eastman JA. Enhancing thermal conductivity of fluids with nanoparticles. IL (United States): Argonne National Lab; 1995.
[18] Kulkarni DP, Das DK, Vajjha RS. Application of nanofluids in heating buildings and reducing pollution. Appl Energy. 2009;86(12):2566–73.
[19] Ramezanizadeh M, Nazari MA, Ahmadi MH, Açıkkalp E. Application of nanofluids in thermosyphons: a review. J Mol Liq. 2018;272:395–402.
[20] Ebrahimnia-Bajestan E, Moghadam MC, Niazmand H, Daungthongsuk W, Wongwises S. Experimental and numerical investigation of nanofluids heat transfer characteristics for application in solar heat exchangers. Int J Heat Mass Transf. 2016;92:1041–52.
[21] Li B, Li C, Zhang Y, Wang Y, Jia D, Yang M, et al. Heat transfer performance of MQL grinding with different nanofluids for Ni-based alloys using vegetable oil. J Clean Prod. 2017;154:1–11.
[22] Hamid M, Usman M, Zubair T, Haq RU, Wang W. Shape effects of MoS2 nanoparticles on rotating flow of nanofluid along a stretching surface with variable thermal conductivity: A Galerkin approach. Int J Heat Mass Transf. 2018;124:706–14.
[23] Alkanhal TA, Sheikholeslami M, Usman M, Haq RU, Shafee A, Al-Ahmadi AS, et al. Thermal management of MHD nanofluid within the porous medium enclosed in a wavy shaped cavity with square obstacle in the presence of radiation heat source. Int J Heat Mass Transf. 2019;139:87–94.
[24] Usman M. Differential transform method for unsteady nanofluid flow and heat transfer. Alex Eng J. 2018;57(3):1867–75.
[25] Usman M. Thermal and velocity slip effects on Casson nanofluid flow over an inclined permeable stretching cylinder *via* collocation method. Int J Heat Mass Transf. 2018;122:1255–63.
[26] Usman M. Novel modification in wavelets method to analyze unsteady flow of nanofluid between two infinitely parallel plates. Chin J Phys. 2020;66:222–36.
[27] Imran M. Heat and mass transport of differential type fluid with non-integer order time-fractional Caputo derivatives. J Mol Liq. 2017;229:67–75.
[28] Caputo M, Fabrizio M. A new definition of fractional derivative without singular kernel. Progr Fract Differ Appl. 2015;1(2):1–13.
[29] Ikram MD. Effects of hybrid nanofluid on novel fractional model of heat transfer flow between two parallel plates. Alex Eng J. 2021;60(4):3593–604.
[30] Atangana A, Baleanu D. New fractional derivatives with non-local and non-singular kernel: theory and application to heat transfer model. arXiv preprint arXiv:1602.03408; 2016.
[31] Saqib M, Khan I, Shafie S. Application of Atangana–Baleanu fractional derivative to MHD channel flow of CMC-based CNT's nanofluid through a porous medium. Chaos Solitons Fractals. 2018;116:79–85.
[32] Wang F. Comparative study of heat and mass transfer of generalized MHD Oldroyd-B bio-nano fluid in a permeable medium with ramped conditions. Sci Rep. 2021;11(1):1–32.
[33] Hassan M. Impact of iron oxide particles concentration under a highly oscillating magnetic field on ferrofluid flow. Eur Phys J Plus. 2018;133(6):1–14.
[34] Hassan M. Effects of iron nanoparticles' shape on convective flow of ferrofluid under highly oscillating magnetic field over stretchable rotating disk. J Magnetism Magnetic Mater. 2018;465:531–9.
[35] Hussain A, Ghafoor S, Malik MY, Jamal S. An exploration of viscosity models in the realm of kinetic theory of liquids originated fluids. Results Phys. 2017;7:2352–60.
[36] Farooq U. Transpiration and viscous dissipation effects on entropy generation in hybrid nanofluid flow over a nonlinear radially stretching disk. Entropy. 2018;20(9):668.
[37] Ullah H, Hayat T, Ahmad S, Alhodaly MS. Entropy generation and heat transfer analysis in power-law fluid flow: Finite difference method. Int Commun Heat Mass Transf. 2021;122:105111.
[38] Khan MI, Kadry S, Chu Y, Waqas M. Modeling and numerical analysis of nanoliquid (titanium oxide, graphene oxide) flow viscous fluid with second order velocity slip and entropy generation. Chin J Chem Eng. 2021;31:17–25.
[39] Khan I. Convective heat transfer in drilling nanofluid with clay nanoparticles: applications in water cleaning process. BioNanoScience. 2019;9(2):453–60.
[40] Anwar T. Generalized thermal investigation of unsteady MHD flow of Oldroyd-B fluid with slip effects and Newtonian heating; a Caputo-Fabrizio fractional model. Alex Eng J. 2022;61(3):2188–202.
[41] Maripala S, Naikoti K. Joule heat parameter effects on unsteady MHD flow over a stretching sheet with viscous dissipation and heat source. Appl Appl Math An Int J (AAM). 2019;14(4):4.
[42] Tahir M. Wall slip and non-integer order derivative effects on the heat transfer flow of Maxwell fluid over an oscillating vertical plate with new definition of fractional Caputo-Fabrizio derivatives. Results Phys. 2017;7:1887–98.
[43] Yusuf T. Irreversibility analysis of Cu-TiO_2-H_2O hybrid-nanofluid impinging on a 3-D stretching sheet in a porous medium with nonlinear radiation: Darcy-Forchheimer's model. Alex Eng J. 2020;59(6):5247–61.
[44] Qing J. Entropy generation on MHD Casson nanofluid flow over a porous stretching/shrinking surface. Entropy. 2016;18(4):123.

[45] Ali Akgül, Asjad MI. Power law memory of natural convection flow of hybrid nanofluids with constant proportional Caputo fractional derivative due to pressure gradient. Pramana. 2020;94(1):1–11.
[46] Zhuang P, Liu F. Implicit difference approximation for the time fractional diffusion equation. J Appl Math Comput. 2006;22(3):87–99.
[47] Sarojamma G, Vajravelu K, Sreelakshmi K. A study on entropy generation on thin film flow over an unsteady stretching sheet under the influence of magnetic field, thermocapillarity, thermal radiation and internal heat generation/absorption. Commun Numer Anal. 2017;2:141–56.
[48] Esfahani J. Influences of wavy wall and nanoparticles on entropy generation over heat exchanger plat. Int J Heat Mass Transf. 2017;109:1162–71.